Conformation of Myosin Interdomain Interactions during Contraction: Deductions from Muscle Fibers Using Polarized Fluorescence†

Thomas P. Burghardt,* Angel R. Cruz-Walker,‡ Sungjo Park, and Katalin Ajtai

Department of Biochemistry and Molecular Biology, Mayo Foundation, 200 First Street SW, Rochester, Minnesota 55905

Received October 16, 2000; Revised Manuscript Received January 4, 2001

ABSTRACT: Myosin cross-bridge subfragment 1 (S1) is the ATP catalyzing motor protein in muscle. It consists of three domains that catalyze ATP and bind actin (catalytic), conduct energy transduction (converter), and transport the load (lever arm). Force development during contraction is thought to result from rotary lever arm movement with the cross-bridge attached to actin. To elucidate cross-bridge structure during force development, two crystal structures of S1 were extrapolated to working "in solution" or oriented "in tissue" forms, using structure-sensitive optical spectroscopic signals from two extrinsic probes. The probes were located at two interfaces containing the catalytic, converter, and lever arm domains of S1. Observed signals included circular dichroism (CD) and absorption originating from S1 in solution in the presence and absence of actin and fluorescence polarization from cross-bridges in muscle fibers. Theoretical signals were calculated from S1 crystal structure models perturbed with lever arm movement from swiveling at three conserved glycines, 699, 703, and 710 (chicken skeletal myosin numbering). Best agreement between the computed and observed signals gave structures showing that actin binding to S1 causes movement of the lever arm. A three-state model of S1 conformation during contraction consists of three actin-bound cross-bridge states observed from muscle fibers in isometric contraction, in the presence of MgADP, and in rigor. Structures best representing these states show that most of the lever arm rotation occurs between isometric contraction and the MgADP states, i.e., during phosphate release. Smaller but significant lever arm rotation occurs with ADP dissociation. Structural changes within the S1 interfaces studied are discussed in the accompanying paper [Burghardt et al. (2001) *Biochemistry 40*, 4834−4843].

Myosin is the energy transducer in muscle, extracting potential energy stored in the structure of the nucleotide ATP and converting it into work. The work production occurs in muscle when myosin interacts with a second protein, actin, to cause relative translation of the two molecules. The crystallographic structures of the myosin proteolytic fragment containing the ATP catalytic site, subfragment 1 (S1),[1] are the basis for elucidating the transduction mechanism. S1 appears to be an articulated molecule made up of three domains that catalyze ATP and bind actin (catalytic), conduct energy transduction (converter), and transport the load (lever arm) (*2*−*7*). The rotating cross-bridge model of contraction (*8*, *9*), modified to accommodate crystallographic and mutagenesis data (*10*), has the lever arm swinging and the catalytic domain bound to actin holding a fixed position during the force generating power stroke of the cross-bridge. Alternative models have the actin playing a more active role in force generation (*11*). Available crystal structures are of S1 without substrate and in nucleotide or nucleotide analogue induced conformations presumed to mimic the real S1 transient states occurring in ATP hydrolysis. Extrapolation of these presumptive transient structures to involve the actin interaction allows investigation of dynamical S1 structure in the contraction cycle. It is in this context that we investigate energy transduction to elucidate its molecular mechanism.

Energy transduction within myosin has features that separate into two categories: one related to action-at-a-distance events where subtle movement at the active site influences distant sites in myosin and the second related to large-scale structural change needed to translate a load. First category features are local conformation changes propagating in myosin along paths through which information and energy flow (*12*). Polypeptide movement causing tryptophan fluorescence enhancement (*13*), actin dissociation, or the forces initiating conserved glycine swiveling demonstrate this information and energy flow. Myosin global conformational changes directly participating in work production, such as the lever arm rotation, are second category features of energy transduction.

Thoughtfully positioned extrinsic spectroscopic probes of myosin offer a look into structural changes accompanying

† This work was supported by National Institutes of Health Grant R01 AR39288 and the Mayo Foundation.

* Corresponding author: phone 507 284 8120; fax 507 284 9349; e-mail burghardt@mayo.edu.

‡ Present address: Department of Chemistry, University of Puerto Rico, Rio Piedras, Puerto Rico 00931.

[1] Abbreviations: AlF_4^-, aluminum fluoride complex; BeF_x, beryllium fluoride complex; CD, circular dichroism; F-S1, 5′-iodoacetamidofluorescein-labeled most reactive thiol in myosin subfragment 1; IAF, 5′-iodoacetamidofluorescein; RLR, reactive lysine residue (Lys84) in myosin subfragment 1; S1, myosin subfragment 1; SH1, most reactive thiol (Cys707) in myosin subfragment 1; TNP-S1, trinitrophenylated reactive lysine residue in myosin subfragment 1; Trp510, ATP-sensitive tryptophan in chicken pectoralis muscle. Myosin sequence numbering throughout the paper is that of chicken pectoralis muscle (*1*).

10.1021/bi002387o CCC: $20.00
Published on Web 03/22/2001

energy transduction that can elucidate both local and global features of the process. The system from which myosin is observed and the spectroscopic signal detected are the available experimental parameters influencing the pertinence of the generated data to local or global S1 conformation. We study myosin assembled into muscle fibers and S1 alone or when it interacts with F-actin in solution. The head portion of myosin oriented in a muscle fiber (cross-bridge) provides a system for deducing the global orientation distribution of probed regions of the cross-bridge. This system is most useful for the sensitive detection of cross-bridge orientation during contraction. Fluorescence polarization detects the global cross-bridge orientation from fluorescent probes while linear dichroism might be used on light absorbing probes that do not fluoresce (*14*, *15*).

S1 alone or in association with F-actin in solution is a randomly oriented system suitable for detection of conformation local to the spectroscopic probe. This system is most useful for the sensitive detection of local S1 structural changes due to interaction with F-actin and/or active site substrate binding. Circular dichroism (CD) detects local probe−protein interactions by producing a structurally interpretable signal originating from the Cotton effect induced in the absorption band of the probe (*16*, *17*). Light absorption supports the CD signal in the characterization of local structure but is usually not structurally interpretable on its own. We describe herein the integration of global and local structure detecting signals from the related muscle systems that constrain possible cross-bridge structures occurring during contraction.

Here, and in the accompanying paper referred to subsequently as part 2 (*18*), we describe and apply the methods for integrating spectroscopic signals from myosin cross-bridges assembled in muscle fibers and from purified S1 free in solution. Accordingly, we find solutions for probe conformation that are consistent with data generated from both systems. Nevertheless, it is convenient to separate the project into two studies: one concerned with the local conformation of S1 and the other with the global positioning of cross-bridges in a muscle fiber. In this paper we are concerned with all things related to the experimental observation of cross-bridge rotation in muscle fibers during contraction and with the practical aspects of how to generate the global position of the cross-bridge in a fiber from the local conformation of the probe in its binding site on S1. Here we will also present our conclusions on global cross-bridge movement during contraction. Part 2 deals with the experimental observation of local S1 conformation from two probes (one of which is our global cross-bridge positioning probe) reporting from two different interfaces among the catalytic, converter, and lever arm domains of S1. These interfacial regions change conformation during energy transduction, dramatically altering the local environments of the probes.

THEORY

We integrate spectroscopic signals from a probe of S1 when the protein is free in solution and when it is part of a muscle fiber cross-bridge. The principal elements for signal integration are the means to compute (i) CD and absorption signals from the probes given the probe/protein coordination and (ii) the fluorescence polarization signals from the fluorescent probes given the probe/protein and protein/F-actin coordinations. The free parameters of the problem are constrained by the available crystallographic data (*2*, *6*), the docking of S1 and F-actin crystal structures (*19*), and the pertinent spectroscopic data. We use general methods introduced by Schellman and co-workers (*20*, *21*) to compute the CD and absorption signals from the S1-bound probes (*22*, *23*). Their application to S1 in solution is the subject of part 2.

We compute the fluorescence polarization signal from a muscle fiber cross-bridge bound probe employing a method different from that used in the past. Our past work integrated angular order information from multiple probes into a common solution for the rotational trajectory of the cross-bridge during contraction (*24*, *25*). There we presumed that all probes moved in rigid coordination with the global movement of the cross-bridge such that data from each probe constrained the same unknown S1 trajectory. The method was linear and highly constrained because each probe provided many more constraints than new unknowns. An articulated cross-bridge, where the lever arm rotates relative to the other domains in the protein, will have probes responding to conformation changes that differ depending on their location in the cross-bridge. In addition, aside from this location-dependent probe movement, our work on the conformation of several probe/protein complexes in S1 indicates that small local movements of the probes due to nucleotide binding are the rule rather than the exception (*22*, *23*). These circumstances are better handled with an approach unifying signals containing local and global conformation information from individual probes.

Polarized Fluorescence and Linear Dichroism. The polarized fluorescence from probe-labeled cross-bridges in muscle fibers senses the orientation of the absorption and emission dipoles in the probe molecule. Linear dichroism senses the orientation of the absorption dipole. We compute the expected polarized fluorescence and linear dichroism from the probe as it assumes allowed orientations relative to the myosin while the protein is docked with an actin filament. The skeletal myosin/actin filament docking coordinates are taken from Mendelson and Morris (*19*). The smooth muscle myosin/actin filament docking coordinates are surmised by alignment of the catalytic domains of skeletal and smooth S1.

Let the actin filament be oriented parallel to the laboratory frame *z*-axis. We adapt the Mendelson and Morris model for one, half-sarcomere cross-bridge orientation distribution in a fiber by ignoring the cross-bridge azimuthal coordinate and evenly distributing the cross-bridge polar and torsional angles inside finite width domains, i.e., inside infinite square well potentials. The docking coordinates are the average angle in each well. This distribution is summed with another one, which is identically constructed but rotated 180° about an axis perpendicular to the actin filament axis, suitable for the second, half-sarcomere cross-bridge orientation distribution. Well widths are adjusted to improve agreement with observations. We choose square wells over Gaussian-shaped domains because square wells lead to analytical, rather than a numerical, expressions for fluorescence intensity and absorption. We allow the probe to undergo independent but restricted rotational Brownian movement relative to the cross-

bridge on a time scale rapid compared to the probe's lifetime. The Brownian probe movement is also restricted by square well potentials.

Experiments were conducted on a microscope or an L-format spectrofluorometer. In the microscope configuration, exciting and collected emitted light propagates along the optical axis of the microscope. In the L-format configuration, exciting and collected emitted light propagates at right angles. We compute the fluorescence polarization ratios, $P_{||}$, $P_{\perp}$, $Q_{||}$, and $Q_{\perp}$, and the linear dichroism, ΔA, defined in both configurations by

$$P_{||} \equiv \frac{F_{||,||} - F_{||,\perp}}{F_{||,||} + F_{||,\perp}} \qquad P_{\perp} \equiv \frac{F_{\perp,\perp} - F_{\perp,||}}{F_{\perp,\perp} + F_{\perp,||}} \tag{1}$$

$$Q_{||} \equiv \frac{F_{||,||} - F_{\perp,||}}{F_{||,||} + F_{\perp,||}} \qquad Q_{\perp} \equiv \frac{F_{\perp,\perp} - F_{||,\perp}}{F_{\perp,\perp} + F_{||,\perp}} \tag{2}$$

$$\Delta A \equiv A_{||} - A_{\perp} \tag{3}$$

where $F_{i,j}$ is the fluorescence intensity and A_i the absorbance for exciting (i) and emitted (j) light polarization || or $\perp$ to the actin filament axis. The four polarization ratios are not independent quantities. They are related by

$$Q_{\perp} = \frac{P_{||} + P_{\perp} - Q_{||} - P_{||}P_{\perp}Q_{||}}{1 + P_{||}P_{\perp} - P_{||}Q_{||} - P_{\perp}Q_{||}} \tag{4}$$

Explicit expressions for these observable quantities, derived in the Appendix, were evaluated in Mathematica 4 (Wolfram Research, Champaign, IL) and then converted to a Fortran subroutine. The subroutine computes the observable quantities given the probe/protein and protein/F-actin coordination.

Computed fluorescence polarization ratio and linear dichroism values are compared to those observed from probe modified muscle fibers in the various physiological states. The probe/protein conformation also determines theoretical values for the other spectroscopic signals (rotary and dipole strengths) observed from S1 in solution in comparable physiological states (for instance S1 + F-actin compared with a muscle fiber in rigor). The details for calculating "in solution" signals are described in part 2. The best choice for the probe/protein conformation is decided by minimizing the difference between the computed signals and experimental data.

Relating Muscle Fiber and Solution Conformations of S1. The ability to extrapolate known S1 structures to involve the actin interaction rests on the related premises that (i) actin binding does not perturb the starting crystal structure too much and (ii) conformation changes in actin-bound myosin are associable with the conformation changes in myosin occurring without actin during ATP hydrolysis. The "too much" in premise (i) means more that we can model by swiveling at the three conserved converter domain glycines, 699, 703, and 710, by their Ramachandran angles. The Ramachandran angles for the swiveling glycines range through values roughly consistent with the extent of their swiveling when S1 goes from the "open" to the "closed" conformation defined by the S1 crystallography (*26*). For this narrow range of structures we can attempt a complete survey of the allowed probe conformations in its binding site. Our initial guess for all computed myosin structures is either the open conformation from the crystal structure of skeletal S1 (*2*) or the closed conformation from the crystal structure of $MgADPAlF_4^-$ trapped smooth muscle S1 (*6*).

The actin-bound cross-bridge conformations observable in muscle fibers are no nucleotide (rigor), in the presence of MgADP, isometric active, and low ionic strength relaxed. Rigor and MgADP conformations have evident solution counterparts in S1 + F-actin and S1 + F-actin + MgADP, respectively. Less intuitive are the in solution analogues for isometric active and low ionic strength relaxed cross-bridges. Using premise (ii), we associate these fiber states with two nucleotide analogue inducible S1 solution states. We identify and motivate these associations with the help of the following background on the process of ATP hydrolysis in myosin.

Myosin-catalyzed ATP hydrolysis has the elementary steps:

$$\mathrm{M + ATP \rightleftarrows M^{*}\cdot ATP \rightleftarrows M^{**}\cdot ADP\cdot P_i \rightleftarrows M^{\wedge}\cdot ADP + P_i \rightleftarrows M + ADP + P_i}$$

where M, M*, M**, and M^ represent distinct transient conformational states of myosin (*27*). Nonhydrolyzable nucleotides or nucleotide analogues bound to, or trapped in, S1 induce static conformations associated with these transient intermediates. Crystallographic and solution structural data suggest that the static structures induced by trapped MgADP−AlF_4^- or MgADP−BeF_x mimic the M**·ADP·P_i or M*·ATP intermediates (*3*, *5*, *28*, *29*) while bound MgATPγS or MgADP mimic M*·ATP or M^·ADP (*30*).

The crystallographic structures of S1 indicate that a large lever arm rotation occurs with the M**·ADP·$P_i \rightarrow$ M^·ADP transition (*6*). We associate this conformation change with the work producing lever arm rotation in the cross-bridge. The isometrically contracting muscle fiber has cross-bridges mainly in the state just prior to work production, suggesting their association with M**. The M** conformation is mimicked with $MgADPAlF_4^-$-trapped S1. The low ionic strength relaxed cross-bridge was already closely identified with the M*·ATP intermediate (*31*). The M* conformation is mimicked with $MgADPBeF_x$ trapped or MgATPγS bound S1.

METHODS

Chemicals. 5′-Iodoacetamidofluorescein (IAF) is from Molecular Probes (Eugene, OR). ADP, ATP, dithiothreitol (DTT), α-chymotrypsin, Triton X-100, and phenylmethanesulfonyl fluoride (PMSF) are from Sigma Chemical (St. Louis, MO). All chemicals are of analytical grade.

Solutions. Rigor solution contains 80 mM KCl, 5 mM $MgCl_2$, 2 mM ethylene glycol bis(β-aminoethyl ether)-*N*,*N*,*N*′,*N*′-tetraacetic acid (EGTA), 1 mM DTT, 0.2 mM PMSF, and 5 mM phosphate buffer. Relaxing solution is rigor solution plus 4 mM ATP. MgADP solution is rigor solution plus 4 mM ADP. Low ionic strength (25 mM) relaxing solution is 1 mM ATP, 1 mM EGTA, 3 mM $MgCl_2$, and 5 mM phosphate buffer. Activating solution is relaxing solution with 0.1 mM $CaCl_2$ replacing the EGTA. Glycerinating solution is relaxing solution with 50% glycerol (volume to volume). Skinning solution is relaxing solution containing 0.5% Triton X-100. Labeling solution is relaxing solution without DTT. All solutions are at pH 7.

Preparation and Modification of Myosin Subfragment 1. Rabbit myosin was prepared by a standard method (*32*). S1 was prepared by digesting myosin filaments with α-chymotrypsin (*33*). S1 (10−25 μM) was modified with a 1.2-fold molar excess of IAF for 12 h at 4 °C in 0.2 mM PMSF and 50 mM TES at pH 7.0. Excess dye was removed by gel filtration (Sephadex column, Bio-Rad 10DG) into rigor buffer and then exhaustive dialysis. This procedure produced fluorescein-labeled S1 (F-S1) with 60−70% of the SH1's modified and no detectable nonspecific label (*34*).

Preparation, Modification, and Decoration of Muscle Fibers. Rabbit *psoas* muscle fibers were obtained as previously described (*35*) and kept in glycerinating solution at −15 °C for up to several weeks. Glycerinated fibers were separated into bundles containing 100−200 fibers each, washed for 10 min in relaxing solution, and then transferred to skinning solution for 30 min. Skinned fibers were washed in labeling solution for 10 min to remove Triton X-100 and DTT and then reacted with 120 μM IAF in labeling solution for 30 min. The reaction was stopped with 1 mM DTT and the excess dye washed out with relaxing solution. All fiber treatments were conducted at 4 °C with intense stirring. Approximately 80% of the total intensity emitted from the IAF label in modified fibers originated from the myosin heavy chain while the remaining probe intensity was distributed among actin, myosin light chain 1, and α-actinin in agreement with earlier work (*34*, *36*).

The location of the probe on the myosin heavy chain was evaluated by comparison of the Ca^{2+}- and K^{+}-EDTA ATPase activities of myosin extracted from labeled fibers as described earlier (*37*). The myosin K^{+}-EDTA ATPase activity of the IAF-labeled myosin extracted from the fibers indicates a 0.35 probe/S1 molar ratio and that all of the probe on the myosin heavy chain resides on SH1 in agreement with earlier work (*34*, *36*). Fibers labeled to this degree exhibited a peak isometric active tension of 115 ± 30 kN/m^2 (mean ± SD). Control fibers, identically handled but unmodified, exhibited a peak isometric active tension of 121 ± 40 kN/m^2. These results suggest no significant impairment of isometric tension due to modification of SH1 with IAF.

In some experiments, fiber bundles prepared for labeling were not treated with probe but otherwise handled identically and then dissected into single fibers and decorated in rigor buffer with 1−2 mg/mL F-S1 for 15−30 min at 4 °C. Unbound F-S1 was washed out from the single fibers with rigor or MgADP solution.

L-Format Steady-State Fluorescence Polarization from Labeled Muscle Fibers. Steady-state fluorescence polarization was observed from labeled fibers in rigor, low ionic strength relaxing, MgADP, and isometric active conditions. In L-format experiments, small bundles of two to five labeled glycerinated fibers were mounted in rigor conditions on a stainless steel holder constructed to fit diagonally in a 1 cm cuvette as described previously (*38*). Fibers were oriented with the fiber axis perpendicular to the plane made from the propagation directions of exciting and collected emitted light. Fibers were equilibrated in rigor, low ionic strength relaxing, MgADP, or isometric activating conditions at 6 °C for 2−3 min before data collection. All samples were verified to be in equilibrium or steady state before the start of data collection by observing no time dependence in their fluorescence. Excitation light had a 4 nm bandwidth and was scanned from 300 to 500 nm. Emission was collected at 550 ± 40 nm using a band-pass filter. Experiments were conducted on a SLM 8000 spectrofluorometer (SLM instruments, Urbana, IL).

Microscopic Fluorescence Measurements on Muscle Fibers. Figure 1 shows the time-resolved fluorescence microscope consisting of an inverted epi-illumination microscope to focus excitation light onto the fiber sample and to collect fluorescence and a length/tension controller (L/T) on the microscope stage to apply length transients to the fiber. Different from the instrument as described previously (*39*) are (i) the method producing linearly polarized exciting light and (ii) the simultaneous detection of orthogonally linearly polarized emitted light. Laser illumination is split into two beams with orthogonal linear polarization at the first polarizing beam splitter (PS1). Acoustooptical modulators (AOM) modulate the intensity of the beams that are rejoined at a second polarizing beam splitter (PS2). The AOM's toggle the excitation light between polarizations parallel or perpendicular to the fiber axis. The intensity of the parallel or perpendicular polarized beams is adjusted to be equal at the sample using AOM gain. Orthogonality of the two polarizations of the exciting light is better than 1 part in 100.

Emitted light collected by the objective undergoes two reflections inside the microscope before emerging at the exit port. One reflection bends the emitted beam through 45°, producing a rotation of the polarization components such that light emitted by the fiber with parallel and perpendicular polarization components does not emerge from the exit port polarized horizontally and vertically. The Fresnel Rhombs (FR) compensate this rotation, and the orthogonal polarization components are separated by the analyzing polarizing beam splitter (PS3) for detection in the avalanche photodiodes (AP) (Perkin-Elmer Optoelectronics, Quebec, Canada). The output from the light detectors is converted to analog signals and measured simultaneously with fiber length and tension data.

Microscopic fluorescence intensity measurements on single glycerinated muscle fibers were carried out using the fiber handling procedures described previously (*39*). Single fibers of 2 mm length were mounted on the length/tension controller under rigor conditions. The fiber was relaxed, stretched slightly until passive tension was detectable, and then equilibrated in rigor, low ionic strength relaxing, or MgADP conditions at 6 °C for 2−3 min before data collection. All samples were verified to be in equilibrium before the start of data collection by observing no time dependence in their fluorescence. Excitation light wavelength is 488 nm and emission wavelength is selected $>\sim$520 nm with dichroic/barrier filters.

Steady-state fluorescence polarization was observed first from the fiber in one or several of its static states, and then the fiber was activated. After development of maximal isometric tension steady-state fluorescence polarization measurements were immediately followed by the time-resolved measurements. One time-resolved measurement consisted of a 5 s excitation light exposure of one spot on the fiber, during which time it was subjected to three to five release/stretch cycles. The time-resolved change in the polarized fluorescence intensities $F_{\parallel,\parallel}$, $F_{\parallel,\perp}$, $F_{\perp,\perp}$, and $F_{\perp,\parallel}$ emitted by the SH1-bound fluorescein were recorded simultaneously and continuously in 1 ms time intervals. Polarized light intensities

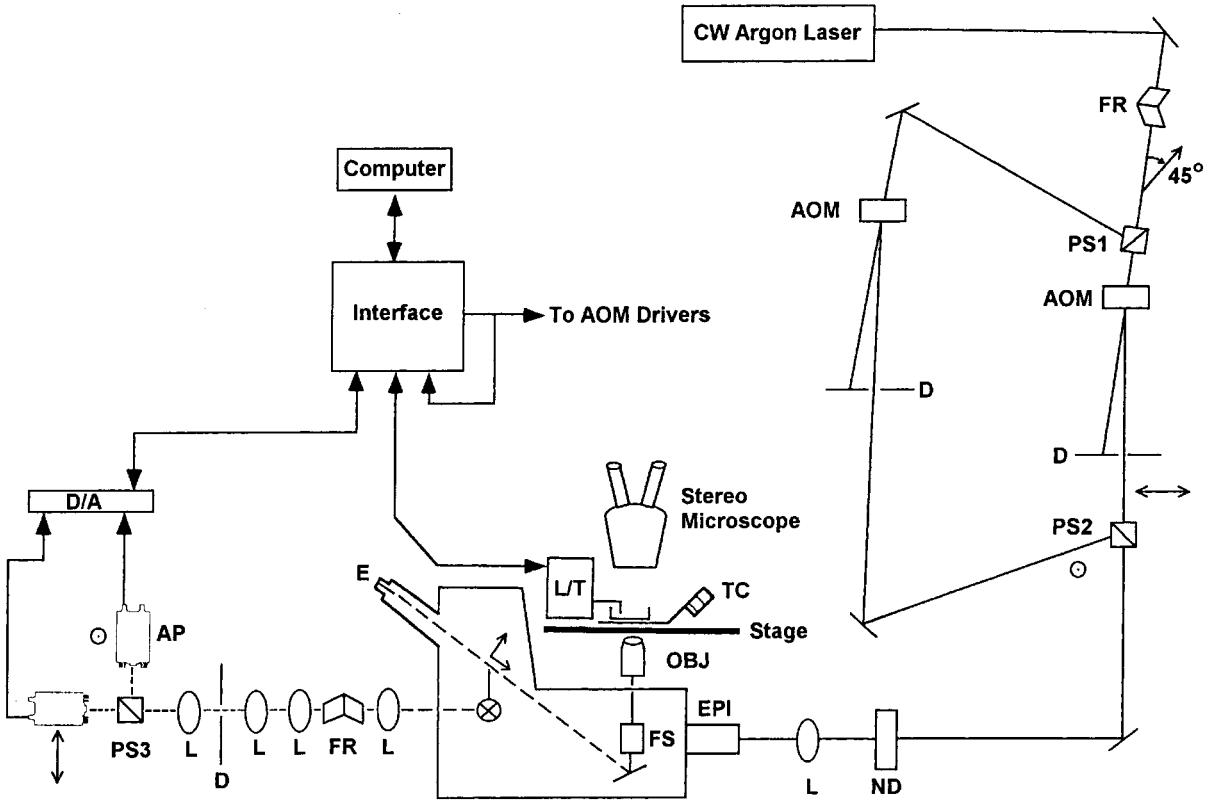

FIGURE 1: Experimental setup for measuring time-resolved intensity changes from fluorescein-labeled cross-bridges in muscle fibers undergoing rapid length transients. Excitation light from an argon ion laser has its linear polarization rotated 45° by a Fresnel Rhombs (FR) polarization rotator which is then split into parallel and perpendicular components at the first polarizing beam splitter (PS1). The two beams are independently intensity modulated by acoustooptical modulators (AOM) and diaphragms (D). The beams are superimposed at PS2, attenuated by a neutral density filter (ND), and focused by a lens (L) before entering the epi-illumination port of an inverted microscope. The filter set (FS) reflects excitation and transmits emitted light. Excitation light is focused to a spot on the sample, and emitted light is collected by the objective (OBJ). Emission propagates to the eyepiece (E) or is directed after a 90° reflection through a camera port (indicated with ⊗) to the photometer unit. The arrows above ⊗ indicate how plane-polarized emitted light parallel or perpendicular to the fiber emerges from the microscope. Relay lenses project the light through the Fresnel Rhombs and a diaphragm. The Fresnel Rhombs return the plane-polarized emitted light to the vertical or horizontal, and the diaphragm rejects out of focus light from the sample. Emitted light is polarization analyzed at PS3. Avalanche photodiodes (AP) detect the parallel and perpendicular polarized intensities. The output from the light detectors are converted to analog signals (D/A) and measured simultaneously with fiber length and tension data from the length/tension controller (L/T). Fibers are mounted with the help of a stereo microscope on a length/tension controller on the stage of the inverted microscope. Sample temperature is controlled by the temperature-controlled stage (TC).

from each stretch/release cycle were signal averaged. The data were stored, and a new spot on the fiber was located using attenuated excitation light. The time-resolved experiments were stopped after 1−2 min of maximal contraction, the fiber was relaxed and rested for 2−3 min, and then the experiment was repeated for up to three times. Fiber length change rates were 0.25−0.5% per 1.5 ms.

To obtain good photon counting statistics, excitation light intensity during the time-resolved experiments was 10−20 times higher than that used for the steady-state measurements. Fluorescein-labeled fibers exhibited fluorescence photobleaching of as much as 10% of the total fluorescence during the 5 s exposure time in a single time-resolved experimental run. We were able to obtain acceptable signal-to-noise levels using the total intensity signal made from the weighted sum of the polarized fluorescence intensities $F_{\parallel,\parallel}$, $F_{\parallel,\perp}$, $F_{\perp,\perp}$, and $F_{\perp,\parallel}$ as defined below.

The total intensity of emitted light, I_T, was computed as described previously (*22*) using the formula

$$I_T \propto {}^1/_2F_{\parallel,\parallel} + F_{\parallel,\perp} + \frac{F_{\perp,\parallel} + {}^4/_3F_{\perp,\perp}}{1 - {}^1/_3\sin^2\omega} \qquad (5)$$

where $\omega \approx 19°$ is the angle between the absorption and emission dipole of fluorescein for 488 nm excitation. Intensity data are presented in normalized form

$$I(t) = \frac{I_T(t)}{\langle I_T(-)\rangle} \qquad (6)$$

where $\langle I_T(-)\rangle$ is the average total intensity before length perturbation.

RESULTS

Steady-State Fluorescence Polarization from Fluorescein-Labeled Muscle Fibers. Table 1 lists the fluorescence polarization ratios measured for fluorescein-labeled muscle fibers in several physiological states. The microscope measurements include data from F-S1-decorated fibers in rigor and in the presence of MgADP conditions. Microscope and L-format observations of $Q_\parallel$ are equivalent by definition and are averaged. $P_\parallel$ for these configurations are also equivalent, but because of fiber symmetry for rotation about the fiber axis, and are averaged. Microscopic and L-format observations of $P_\perp$, referred to subsequently as $P_\perp$ and $P_\perp^L$,

Table 1: Microscope, L-Format, and Computed Fluorescence Polarization Ratios from Fluorescein-Labeled Muscle Fibers

	Microscope[a]					
myosin label[b]	$P_{\|\|}$		$P_\perp$		$Q_{\|\|}$	
	intrinsic	exogenous	intrinsic	exogenous	intrinsic	exogenous
rigor	0.31	0.15	0.29	0.43	0.32	0.22
MgADP	0.46	0.52	0.24	0.25	0.44	0.51
low μ relax[c]	0.43		0.30		0.42	
active[c]	0.40		0.33		0.40	

	L-Format[d]		
	$P_{\|\|}$	$P_\perp^L$	$Q_{\|\|}$
rigor	0.27 ± 0.02	-0.10 ± 0.01	0.22 ± 0.02
MgADP	0.44 ± 0.01	-0.15 ± 0.01	0.38 ± 0.01
low μ relax	0.41 ± 0.01	-0.12 ± 0.02	0.37 ± 0.02
active	0.38 ± 0.01	-0.09 ± 0.01	0.33 ± 0.01

	Computed[e]				
	$P_{\|\|}$	$P_\perp$	$P_\perp^L$	$Q_{\|\|}$	$(\epsilon_3 - \epsilon_1)/\epsilon$
rigor	0.12	0.22	−0.11	0.19	0.12
MgADP	0.13	0.24	−0.13	0.54	0.96
low μ relax	0.11	0.26	−0.10	0.46	0.75
active	0.20	0.19	−0.22	0.53	0.96

[a] Standard error of the mean is ≤0.01 with the number of observations ≥5 for each ratio listed. Excitation wavelength was 488 nm and emission was collected at >∼520 nm. [b] The moiety that carries the IAF is the cross-bridge assembled in the thick filament of the fiber (intrinsic) or F-S1 decorating fibers (exogenous). [c] F-S1 dissociates rapidly from decorated fibers in low ionic strength relaxed or active conditions prohibiting polarization ratio observation. [d] Errors are standard error of the mean for four observations. Excitation wavelength was 488 nm and emission was collected at 550 ± 40 nm. [e] Restricted independent movement of the fluorescein probe was modeled as the free rotational diffusion of fluorescein in a square well potential. Two degrees of freedom, corresponding to the polar and torsional rotational motion of the probe's instantaneous molecular frame, were modeled as described in the Appendix. Best results were found with equal polar and torsional square well widths of 12°. The heading $(\epsilon_3 - \epsilon_1)/\epsilon$ corresponds to the linear dichroism signal defined in eq 20a. There are no experimental data for this parameter.

are independent. A data set for a cross-bridge bound probe in a particular physiological state consists of the four quantities $P_{\|}$, $Q_{\|}$, $P_\perp$, and $P_\perp^L$.

IAF-modified muscle fibers have ∼80% of the probe molecules localized at SH1 while the rest modifies actin, myosin light chain 1, and α-actinin, as indicated in Methods. This level of specificity is equivalent to that of 5′-iodoacetamidotetramethylrhodamine (5′IATR) modified fibers (*36*). IAF modifies essentially only SH1 in the purified S1 used to decorate fibers in rigor and MgADP conditions. The significant contrast in the polarization ratios between IAF-labeled and F-S1-decorated fibers, approximately equivalent to that observed for 5′IATR under the same circumstances (data not shown), originates from dispersion in cross-bridge ordering due to strain and from the nonspecific probes in labeled fibers. The polarization ratios are used to establish a best estimate for the orientation of the probe at SH1 assuming dispersion in the cross-bridge order influencing a signal that originates only from this site. Given the foregoing, we used the decorated fiber data in preference to the labeled fiber data when possible.

Effect of Length Transients on Fluorescein Fluorescence in Muscle Fibers. Figure 2 shows the time course of normalized fluorescence intensity, $I(t)$, and tension per unit area, F/A, in kN/m^2, for IAF-labeled fibers in isometric active contraction (■) and relaxation (□). The fractional percent change in fiber length, $\Delta L/L \approx 0.5\%$, is identical for contraction and relaxation experiments. Both normalized light intensity traces show no effect due to the length transient. Decreasing $\Delta L/L$ to ∼0.25% did not influence the behavior of $I(t)$ (data not shown). The result in relaxation is expected for a normally detached cross-bridge and was observed previously (*22*).

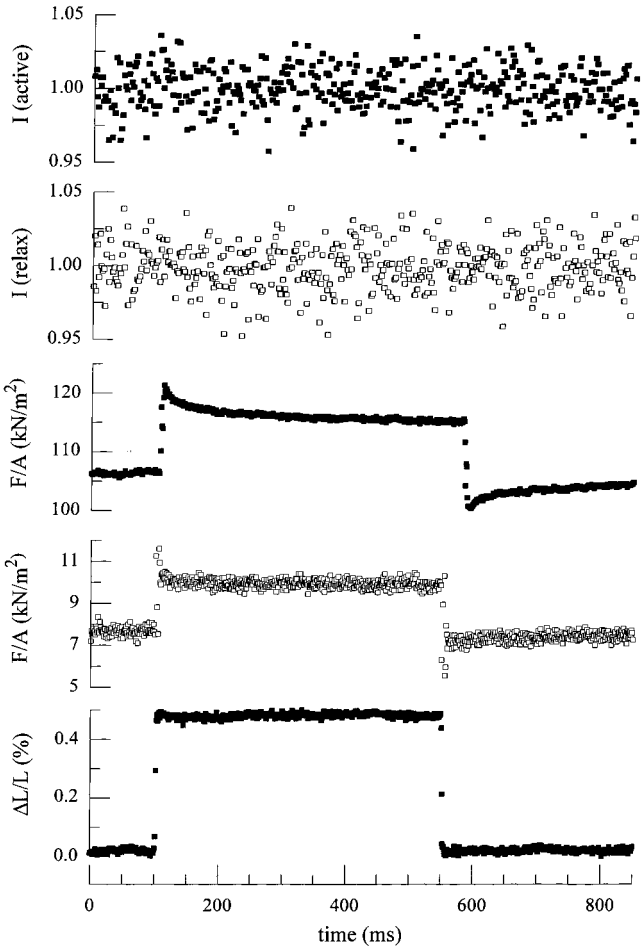

FIGURE 2: Time course of normalized fluorescence intensity, I, and tension per unit area, F/A, for IAF-labeled fibers in isometric active contraction (■) and relaxation (□) during length transients. The fractional percent fiber length change, $\Delta L/L$, is identical for contraction and relaxation experiments.

Previously, in related experiments, normalized fluorescence intensity from IAF-labeled cross-bridges in rigor fibers was shown to change in response to length transients (*22*). There, emission intensity reversibly decreased upon stretching the fiber, demonstrating that strain on a labeled rigor cross-bridge could induce a change in IAF fluorescence. Fluorescence from F-S1 is known to increase substantially upon formation of the rigor bond with actin (*40*). This effect was attributed to the withdrawal of a nearby quenching residue when S1 changes conformation upon binding actin. It seems likely that straining the rigor cross-bridge with a length transient likewise modulates the proximity of this quencher to IAF. Our results on the IAF/S1 conformation, discussed below and in part 2, are consistent with the notion that the quenching group is indole from Trp510.

Unlike the effect on a rigor cross-bridge, we now find that the length transient on active cross-bridges does not measur-

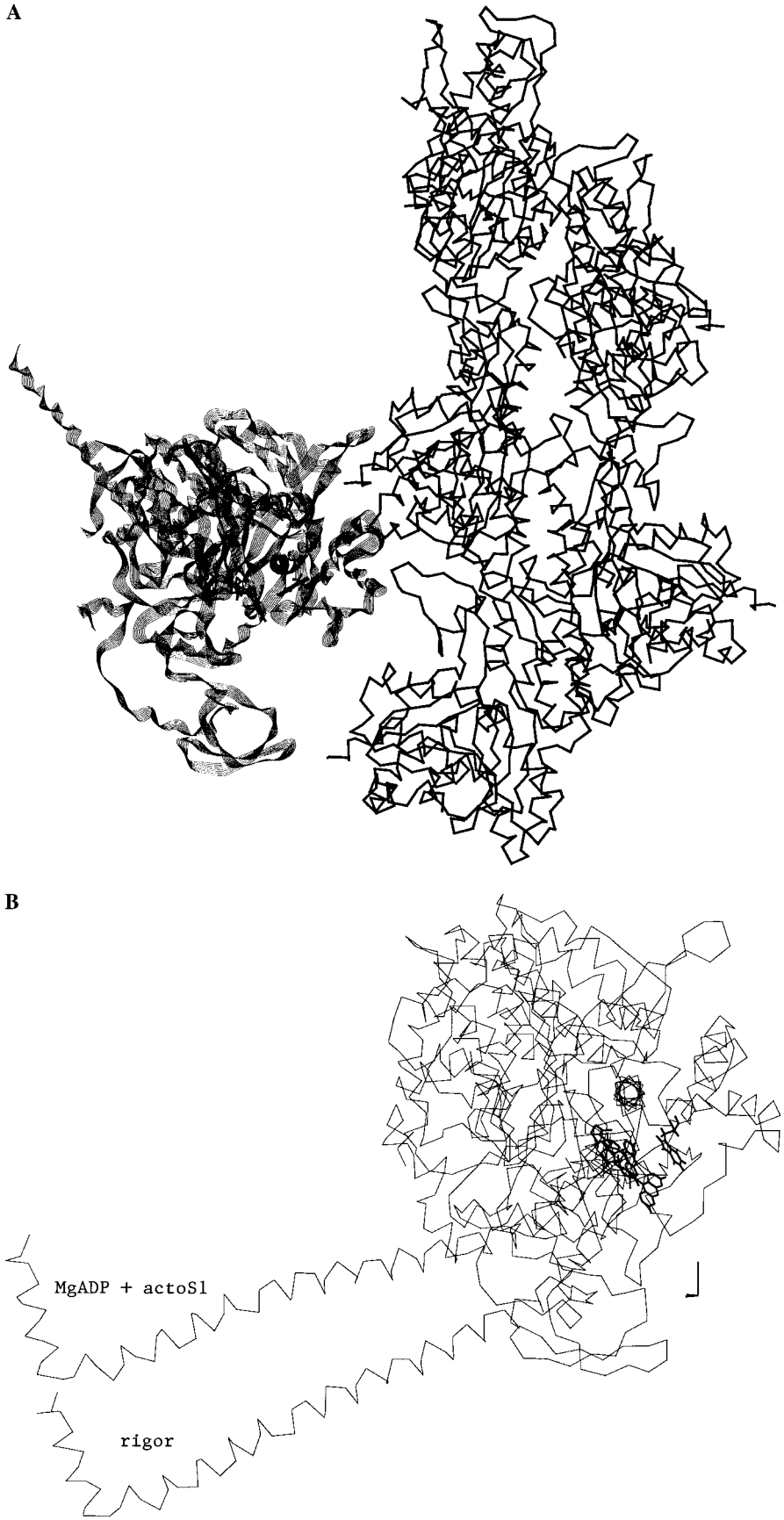

FIGURE 3: Myosin cross-bridge docked with F-actin. All views show the lever arm in the foreground looking down the symmetry axis of the switch-2 helix. (A) Ribbon diagram of smooth muscle myosin bound to actin representing the isometrically active cross-bridge. F-actin is represented by the α-carbons of G-actin arranged in a polymer-like assembly (*19*). (B) α-Carbon diagram of skeletal muscle myosin bound to actin representing the MgADP (upper lever arm) and rigor cross-bridges. Bolded atoms are from IAF (in the rigor or MgADP state) and from Trp510. The actin filament is not shown but would appear as in (A) with the filament axis parallel to the long coordinate axis in the lower right corner.

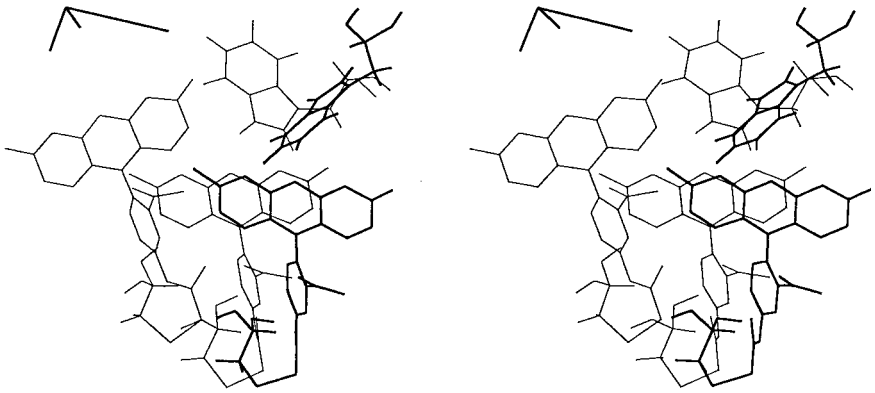

FIGURE 4: Stereoview of the translation and rotation of IAF while attached to SH1 and Trp510 when the cross-bridge assumes the rigor, MgADP, and isometrically active (bolded) conformations in a muscle fiber. The probe moves from left to right in these conditions. Trp510 has the same conformation in both the rigor and MgADP states. The actin filament in a muscle fiber is parallel to the long coordinate axis in the upper left corner.

ably influence emission from IAF at SH1. Cross-bridges in an isometric active fiber predominantly populate an actin-bound state just prior to the power stroke. A rapid short-length change allowing the fiber to shorten transiently reduces tension (see Figure 2). Tension recovery follows as synchronous cross-bridges populate lower free-energy actin-bound states without detachment (*9*). Depletion of the predominant state and population of the lower free energy actin-attached states would be detected by IAF fluorescence if the IAF/S1 conformation changes among these actin-attached states to modulate proximity of the IAF quencher. Barring the possibility that the rapid length change perturbation of the cross-bridge conformation distribution in isometric active fibers produces a variety of intensity changes in IAF that exactly compensate each other, it would seem that all of the actin-attached states occupied during tension recovery maintain a similar distance (but shorter than in rigor) between IAF and its quencher in S1. Consequently, the concentration of the rigor component in the actin-attached states, averaged over the observed 1 ms time intervals, is undetectable.

Conformation of the Myosin Cross-Bridge. The best choices for the local and global probe/protein conformations were decided by minimizing the difference between the computed signals and experimental data. Adjustable parameters were dihedral angles conforming the modified side chain and probe to its binding site, each probe had an independent set of these parameters, and the Ramachandran angles for the conserved glycines 699, 703, and 710. The Ramachandran angles were identical for probes under equivalent physiological conditions. Experimental observations from the fluorescein probe at SH1 consisted of fluorescence polarization from muscle fibers and CD and absorption data from F-S1 in solution in the presence and absence of F-actin. Experimental observations from S1 with trinitrophenylated RLR (TNP-S1) consisted of CD and absorption data from TNP-S1 in solution in the presence and absence of F-actin. The one exception was isometric active cross-bridges modeled using smooth muscle myosin. For this case we compared observed and computed fluorescence polarization signals from IAF at SH1 but did not attempt to fit the other spectroscopic data all taken from rabbit myosin S1. The CD and absorption data are presented in part 2. Figures 3−6 summarize selected best choices for S1 conformations.

Cross-Bridge Conformation during Force Production in Contraction. Figure 3 shows a ribbon diagram of the myosin cross-bridge docked with F-actin in states representing those present during force production in a contracting muscle fiber. The actin polymer is shown explicitly only in Figure 3A. In Figure 3B F-actin would appear as in Figure 3A with the polymer axis vertical and parallel to the long coordinate axis shown in the lower right corner. Figure 3A shows the isometrically active cross-bridge. The lever arm is poised to begin the power stroke. The view shows SH1-bound fluorescein, Trp510, and the lever arm in the foreground looking down the axis of the helix formed by residues 475−509 (the switch-2 helix) (*26*).

Figure 3B shows the superposition of skeletal myosin cross-bridges in the presence of MgADP and in rigor from a view identical to that in Figure 3A. The two structures overlap from the N-terminus to Gly699. At Gly699 and further downstream the structures diverge due to swiveling at the conserved glycine residues 699, 703, and 710. The upper lever arm is from the MgADP structure. Two fluorescein molecules are indicated because their point of attachment to myosin at SH1 undergoes rotation and translation upon MgADP binding to the active site.

Figure 4 shows a stereoview of the translation and rotation of Trp510 and IAF while attached to SH1 when the cross-bridge assumes the rigor, MgADP, and isometrically active conformations in a muscle fiber (probe moves sequentially from left to right). In this view the actin filament in a muscle fiber is parallel to the long coordinate axis in the upper left corner and the bolded conformation corresponds to the isometrically active cross-bridge. Trp510 is in the identical position for the rigor and MgADP conformations. MgADP and isometrically active probe conformations are similar but not identical, differing by a significant rotation of the probe dipole as observed previously (*39*). The rigor probe conformation is very different from the others belying the obvious, that the major protein conformational change occurs between isometrically active and either of the other fiber states (compare conformations in panels A and B of Figure 3).

Figure 5 shows the cross-bridge in the presence of MgADP near the lever arm and converter domains as in Figure 3B but from a different viewpoint. Trinitrophenylated RLR (double-labeled probes were not used experimentally) and the side chain interacting with TNP, Arg723, are also shown.

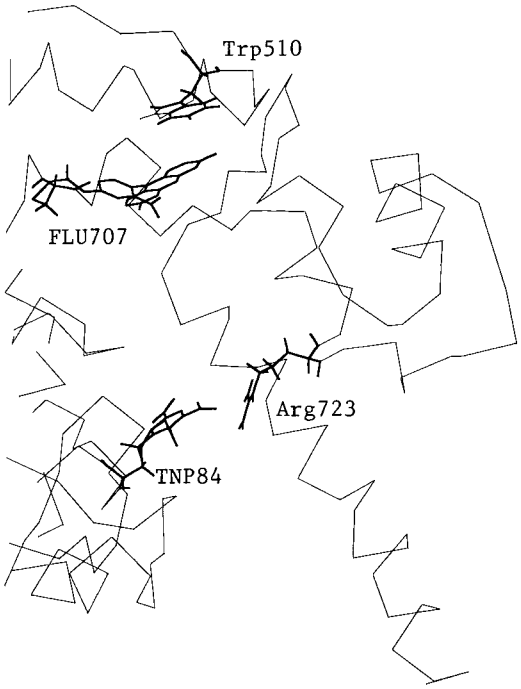

FIGURE 5: Actin-bound S1 in rigor as in Figure 3B from a different viewpoint, with trinitrophenylated RLR and the side chain interacting with TNP, Arg723. This view isolates the converter and lever arm domains from the catalytic domain and indicates the favorable positions of IAF and TNP for detecting changes in the conformation of interdomain interactions.

IAF, Trp510, TNP, and Arg723 are bolded. The view in Figure 5 isolates the converter/lever arm domains from the rest of the S1, showing the favorable positions of IAF and TNP for detecting their movement relative to the catalytic domain.

Figure 6 illustrates the effect of actin binding on S1 conformation. Shown is the superposition of skeletal S1 + MgADP + F-actin (identical to that in Figure 3B) with S1 + MgADP. The view of the molecules is identical to that in Figure 3. The lever arm displacement is similar to that seen in Figure 3B where S1 + MgADP + F-actin and rigor states are compared. The direct comparison of the S1 + MgADP and rigor conformations (not shown) shows they differ by a 10 Å displacement of the C-terminus caused by a 5−6° rotation of the lever arm about the actin filament axis.

DISCUSSION

The extrapolation of solid-state myosin S1 structures to working native "in solution" or "in tissue" structures is a challenging problem facing investigators seeking to understand the molecular mechanisms underlying energy transduction in muscle contraction. While an S1 solution structure from nuclear magnetic resonance (NMR) may one day be possible, for now the size and complexity of S1 is prohibitive. Alternatively, we have undertaken an optical spectroscopic approach that is feasible and informative but certainly less definitive than NMR. Nonetheless, we maximally exploit the information content of the spectroscopic signals by focusing attention on two interesting regions within S1 using two site-specific extrinsic probes (Figure 5). These probed regions are interfaces among the catalytic, converter, and lever arm domains. We also use one of the probes in different experimental modes that distinguish local probe/protein interactions from the more global picture indicated by probe orientation in space.

Working Model for Energy Transduction. The CD, absorption, and fluorescence polarization signals, obtained from one or more extrinsic probes of S1 and appropriately combined, provide insufficient constraints to make an unambiguous structure determination. By combining these spectroscopic data with the available S1 crystal structures and inventing a method to model the structural perturbations of S1 caused by ATP hydrolysis and/or actin binding, we can propose transient S1 and actoS1 structures that satisfy the available constraints. We call this a working model of energy transduction because it addresses structural changes but not the underlying mechanism in the process. The proposed structures are approximations to S1 transients that will be refined in the future using the more diverse set of crystal structures that will inevitably become available and better (functional) models for energy transduction. The main postulate in this approach is the energy transduction model providing the guesses for S1 transients bridging the known crystal structures. Practical considerations dictate that we cannot assign a free parameter to every atomic degree of freedom in the S1 molecule (that approach would be model free but lacking in concept) so the model must be simplifying but simultaneously consistent with the optical spectroscopic constraints. Lever arm swinging is the most remarkable conformation change identified by the crystal structures of S1, and swiveling at the three conserved glycines, 699, 703, and 710, conveniently reproduces this feature. Furthermore, these glycines are conserved in all known myosin sequences (except Gly703 that is conserved within the myosin II class only) and were shown to be necessary for myosin functionality (*41*, *42*).

The three-swivel model of S1 structural dynamics has limitations. It is insufficient to bridge the "closed" and "open" forms of the S1 crystal structures because there are significant delocalized differences between them. The transition between closed and open forms, corresponding to the M** → M^ transition, is thought to be the power stroke in muscle contraction (*26*). The open forms of myosin (M, M*, or M^) have several crystallographic representations (*2*−*4*), and we find that the transitions among them are adequately handled with the three-swivel model of S1 structural dynamics. The closed form has one available representation from smooth muscle myosin (*6*). A way out of this dilemma is to wait for the structure of one or more intermediates between the closed and open forms to be solved to guide us along the conformational path joining the end points hopefully with individually simpler, more localized, conformation changes. Another more expedient idea is to simply adopt the closed form structure from the smooth muscle and see if it can account for spectroscopic data observed from rabbit skeletal S1. We tried the latter. After docking the smooth muscle S1 to F-actin and allowing conformational change using the three-swivel model, the protein coordinates oriented fluorescein at SH1 to produce good agreement between computed and observed fluorescence polarization ratios. The observed polarization ratios were those of an isometric active fiber. We did not attempt to account for the CD and absorption data from rabbit S1 with the smooth muscle model thinking that any outcome from such a detailed comparison is not necessarily informative.

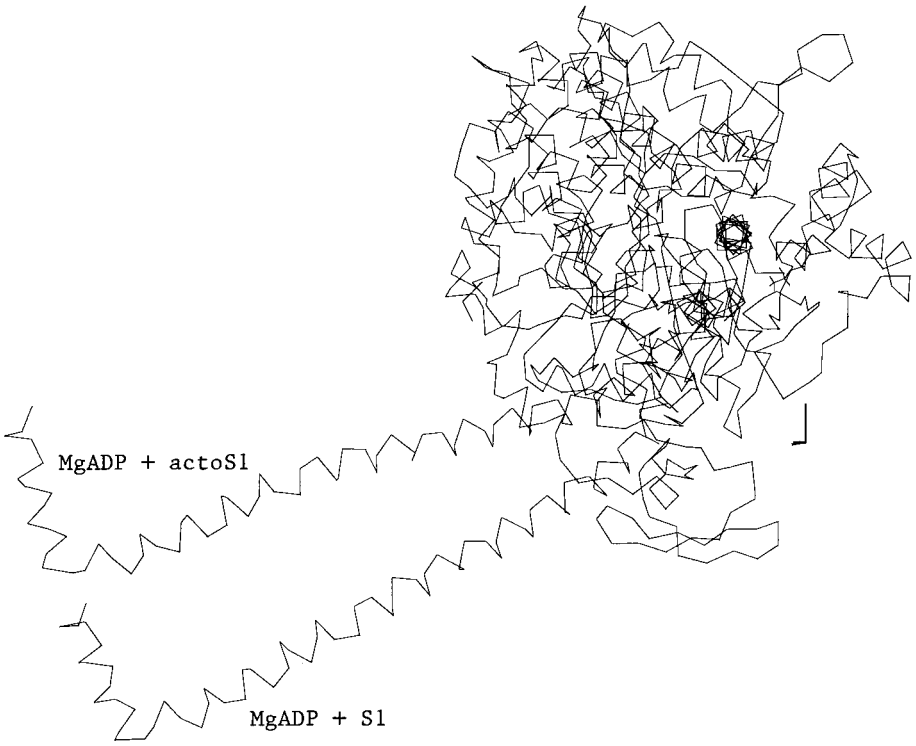

FIGURE 6: Actin-induced structural change in the MgADP−S1 complex. Superimposed are skeletal MgADP + actoS1 and MgADP + S1 from a view identical to that in Figure 3. The actin polymer axis is vertical and parallel to the long coordinate axis in the lower right corner.

Actin Binding Effect. Our association of S1 and actoS1 conformations with the M, M*, M**, and M^ structural forms is overly simplistic because it ignores one of the main findings presented here, that actin binding perturbs S1 structure. We find that actin binding causes structural changes in S1 that are adequately handled by the three-swivel model and that it principally causes movement of the lever arm. Figure 6 shows the actin binding effect on S1 in the presence of MgADP.

Dynamical Cross-Bridge Structure during Force Development. A model for unitary force generation in muscle contraction has the myosin cross-bridge changing conformation while firmly attached to actin. A simple representation of cross-bridge force generation consists of three actin-bound cross-bridge states observed from muscle fibers in isometric contraction, in the presence of MgADP, and in rigor, going from highest to lowest free energy. Panels A and B of Figure 3 show these structures representing force generation in a fiber. We found that the largest movement of the lever arm occurs with the isometric active → MgADP state transition, displacing the projection of the C-terminus of skeletal S1 on the actin filament ∼100 Å. Additionally, the MgADP → rigor state transition further rotates the lever arm, causing an actin projected C-terminus displacement of ∼20 Å. The ∼120 Å step size was anticipated from the S1 crystal structures on the basis of the large difference in the lever arm domain orientation between skeletal and $MgADPAlF_4^-$-trapped smooth muscle S1's (*6*).

SH1-Bound Fluorescein Conformation during Contraction. Whether or not probes attached to SH1 in skeletal muscle fibers rotate when fibers developed force has been controversial (*39*, *43*). The results in Figure 3 give a quantitative accounting of IAF movement at SH1. IAF-labeled SH1 rotates as the cross-bridge develops force, as suggested previously from time-resolved fluorescence polarization measurements from a similar probe at this site (*39*). This conclusion is not surprising since it was anticipated from comparison of the crystal structures for skeletal S1 with that from $MgADPAlF^-_4$-trapped smooth muscle S1 (*6*) and from the crystallographic studies of truncated *Dictyostelium* S1 (*44*). Figure 4 clarifies the issues for the xanthene dyes. There it is seen that the smaller probe rotation and displacement accompany the larger S1 conformation change as the cross-bridge accomplishes the bulk of the power stroke when it moves from the isometrically active to the MgADP conformation. Then the larger probe rotation and displacement accompany the smaller S1 conformation change as the cross-bridge releases MgADP. The counterintuitive inverse correlation of cross-bridge and probe movement fostered a situation where significant probe rotation was overlooked. This scenario was suggested previously following the analysis of data from multiple spin and fluorescent probes of SH1 (*24*, *25*).

Figure 4 also indicates that IAF moves away from Trp510 as the cross-bridge makes the MgADP to rigor structural transition in fibers. This movement changes the average distance from the xanthene of fluorescein to the Trp510 indole from 5.8 to 8.6 Å. Ando observed the fluorescence from IAF modifying SH1 to undergo a significant enhancement when S1 forms the rigor bond and suggested that a fluorescein quenching group in S1 must withdraw from the vicinity of the xanthene upon formation of the rigor bond (*40*). The 5.8 Å separation between xanthene and indole in the MgADP state is more than 2 Å too far for typical charge-transfer quenching (*45*); however, the trend that in rigor the groups become more distant agrees with Ando's hypothesis if Trp510 is the fluorescein quenching group. In related work, we observed SH1-bound fluorescein quenching in rigor muscle fibers that are subjected to length transients such that stretching the fiber quenches the fluorescein (*22*). If the rigor

cross-bridge is at the end of the power stroke, then we might expect, as have others before us (*46*, *47*), that stretching a fiber in rigor should reverse the cross-bridge conformation changes leading to force generation. In view of the results in Figure 4 it would seem that the reversal of the cross-bridge conformation changes leading to force generation would move the IAF closer to Trp510, thereby increasing the probability for fluorescein quenching. Thus our findings are consistent with the notion that pulling a rigor fiber can at least partially reverse the power stroke insofar as the movement of SH1 is concerned.

Implications for Fluorescence Polarization from Probes Embedded in Proteins. The computation of the fluorescence polarization from a probe embedded in a protein when the protein is oriented in space proceeds according to the method summarized in the Appendix. Evidently the polarization ratios depend ultimately on the orientation in space of the probe electric dipole moment. Complicating the issue are the coupled local fields contributed by the protein host that influence, we find sometimes dramatically, the orientation of the probe electric dipole. We observed this phenomenon with the fluorescein probe in its binding site on S1. The orientation of the absorption and emission dipoles of fluorescein were at times strongly influenced by probe/S1 contacts and in particular by the IAF/Trp510 coordination. This is not surprising given the well-established fluorescein sensitivity in F-S1 to the form of the active site substrate or to actin binding suggesting S1 exerts significant influence on IAF (*40*, *48*). In general, it should be recognized that the probe dipole moment orientation can be perturbed significantly by interaction with the local fields in the protein binding site.

Conclusions. Solid-state myosin S1 structures were extrapolated to working "in solution" or oriented "in tissue" forms by comparing observed structure-sensitive optical spectroscopic signals from extrinsic probes located at two different interfaces within S1 containing the catalytic, converter, and lever arm domains. Computed signals were generated from skeletal or smooth muscle S1 crystal structures by perturbing them using a simple working model of energy transduction. We found that actin binding to S1 always causes movement of the lever arm domain and summarized S1 conformation dynamics during force development in contraction in three snapshots. During force development most (5/6) of the lever arm displacement occurs with phosphate release before ADP dissociation. The remainder (1/6) occurs when ADP dissociates from the active site of myosin.

ACKNOWLEDGMENT

We thank Ms. S. P. Garamszegi for technical assistance on the project.

APPENDIX

Fluorescence Polarization and Linear Dichroism from a Probe of the Myosin Cross-Bridge. In a fluorescence experiment excitation light propagates from the laboratory $+y$-axis toward a sample at the origin. Emission collection is from along the $+y$-axis (microscope format) or the $+x$-axis (L-format). Linear dichroism has the microscope geometry but with incident light propagating from the laboratory $-y$-axis. The laboratory x-, y-, and z-axes are referred to subsequently with indices 1, 2, and 3, respectively. Equations 1a−3a are the polarization ratios and linear dichroism for the microscope format

$$P_{\|} \equiv \frac{F_{3,3} - F_{3,1}}{F_{3,3} + F_{3,1}} \qquad P_{\perp} \equiv \frac{F_{1,1} - F_{1,3}}{F_{1,1} + F_{1,3}} \tag{1a}$$

$$Q_{\|} \equiv \frac{F_{3,3} - F_{1,3}}{F_{3,3} + F_{1,3}} \qquad Q_{\perp} \equiv \frac{F_{1,1} - F_{3,1}}{F_{1,1} + F_{3,1}} \tag{2a}$$

$$\Delta A \equiv A_3 - A_1 \tag{3a}$$

where $F_{i,j}$ is the fluorescence intensity and A_i the absorbance for exciting (i) and emitted (j) light polarization. For the L-format

$$P_{\|} \equiv \frac{F_{3,3} - F_{3,2}}{F_{3,3} + F_{3,2}} \qquad P_{\perp} \equiv \frac{F_{1,2} - F_{1,3}}{F_{1,2} + F_{1,3}} \tag{4a}$$

$$Q_{\|} \equiv \frac{F_{3,3} - F_{1,3}}{F_{3,3} + F_{1,3}} \qquad Q_{\perp} \equiv \frac{F_{1,2} - F_{3,2}}{F_{1,2} + F_{3,2}} \tag{5a}$$

The azimuthal symmetry of the muscle fiber implies equal $P_{\|}$'s in the microscope and L-format experiments. $Q_{\|}$'s are identical for the two configurations (see eqs 2a and 5a) but $P_{\perp}$'s are independent.

Several coordinate frames defined for the probe and the muscle fiber system aid in the derivation of $F_{i,j}$ and A_i. They are defined below. When we speak of probe or protein, it should be understood that the probe is covalently linked to the protein.

Dipole Frame (DF). The frame fixed to the probe molecule where the emission dipole (emission dipole centered) or the lowest energy absorption dipole (absorption dipole centered) is along the z-axis. The choice for the x-axis in the emission dipole centered frame is such that a particular absorption dipole has a $+x$ component. The choice for the x-axis in the absorption dipole centered frame is such that a particular higher energy absorption dipole has a $+x$ component.

Instantaneous Molecular Frame (IMF). The frame fixed to the probe molecule that is convenient for describing its independent but restricted movement relative to the protein. Fluorescein has an IMF with the z-axis in the xanthene plane but perpendicular to the long dimension of the xanthene pointing away from the benzyl group. The x-axis is along the long dimension of the xanthene. The y-axis is perpendicular to the xanthene plane. The rotational diffusion equation governs the independent probe movement.

Average Molecular Frame (AMF). The time- or ensemble-averaged IMF's of the probe. If the probe does not move independently from the protein, then the IMF and the AMF are identical.

Principal Inertial Frame (PIF). The S1 fixed frame where the inertial tensor is diagonal. This is not uniquely defined for S1 because the protein changes conformation during ATP hydrolysis and contraction. We avoid defining PIF's for each transient S1 structure by computing one PIF from heavy chain residues 4−494, roughly corresponding to the catalytic domain. Our working model of dynamic S1 conformation

does not change conformation of this region of S1 during ATPase and force generation.

Laboratory Frame (LF). In the laboratory frame the muscle fiber symmetry axis is parallel to the *z*-axis. Positions of laboratory *x*- and *y*-axes are arbitrary due to fiber symmetry.

Euler rotations relate these coordinate frames. Eu(α,β,γ) is the Euler matrix converting space-fixed coordinates to body-fixed coordinates. It is defined by

$$\mathrm{Eu}(\alpha,\beta,\gamma) = \begin{pmatrix} \cos\gamma & \sin\gamma & 0 \\ -\sin\gamma & \cos\gamma & 0 \\ 0 & 0 & 1 \end{pmatrix} \begin{pmatrix} \cos\beta & 0 & -\sin\beta \\ 0 & 1 & 0 \\ \sin\beta & 0 & \cos\beta \end{pmatrix} \begin{pmatrix} \cos\alpha & \sin\alpha & 0 \\ -\sin\alpha & \cos\alpha & 0 \\ 0 & 0 & 1 \end{pmatrix} \quad (6a)$$

Using the appropriate Euler rotations defined below, all vector quantities are expressed in the IMF to facilitate parametrization of the probe's independent movement. For any vector $\vec{u}$

$$\vec{u}_{PIF} = \mathrm{Eu}(\alpha_c,\beta_c,\gamma_c)\vec{u}_{\mathrm{LF}} \qquad \vec{u}_{\mathrm{AMF}} = \mathrm{Eu}(\alpha_b,\beta_b,\gamma_b)\vec{u}_{\mathrm{PIF}} \quad (7a)$$

$$\vec{u}_{\mathrm{IMF}} = \mathrm{Eu}(\alpha,\beta,\gamma)\vec{u}_{\mathrm{AMF}} \qquad \vec{u}_{\mathrm{IMF}} = \mathrm{Eu}(\phi_1,\theta,\phi_2)\vec{u}_{\mathrm{DF}} \quad (8a)$$

We use subsequently one symbol to denote the three Euler angles, for instance, $\Omega_c = (\alpha_c,\beta_c,\gamma_c)$. From eqs 7a and 8a, any vector known in the LF may be expressed in the IMF with

$$\vec{u}_{\mathrm{IMF}} = \mathrm{Eu}(\Omega)\mathrm{Eu}(\Omega_b)\mathrm{Eu}(\Omega_c)\vec{u}_{\mathrm{LF}} \quad (9a)$$

The dipole moment vector $\vec{\mu}_{\mathrm{DF}}$, known in the dipole frame, is expressed in the IMF using the right equation in (8a). Now we form expressions for fluorescence and absorption.

The independent probe movement is described by a time-dependent probability density $P(\Omega,t)$ that is the solution to the Fokker−Planck equation with boundary conditions (*49*). The initial condition is

$$P(\Omega,t=0) = (\vec{E}_{\mathrm{IMF}}\cdot\vec{\mu}_{\mathrm{a,IMF}})^2 N(\Omega_c) \quad (10a)$$

where $\vec{\mu}_{\mathrm{a,IMF}}$ is the absorption dipole and $N(\Omega_c)$ is the static angular distribution of cross-bridges. If the Fokker−Planck equation is a Sturm-Louisville problem (like free rotational diffusion within limited angular boundaries), the solution for $P(\Omega,t)$ is

$$P(\Omega,t) = N(\Omega_c)\sum_j e^{-\lambda_j t}\psi_j(\Omega)\int_{\Omega_0} d\Omega'[\vec{E}_{\mathrm{IMF}}\cdot\vec{\mu}_{\mathrm{a,IMF}}]^2\psi_j^*(\Omega') \quad (11a)$$

where $\psi_j(\Omega)$'s are complete orthonormal functions on interval Ω_0 satisfying the Fokker−Planck equation with relaxation rates λ_j. The time-averaged fluorescence and absorption are

$$F \propto \int_{\Omega_1} d\Omega_c \int_{\Omega_0} d\Omega \int_0^\infty dt\, e^{-t/\tau}[\vec{n}_{\mathrm{IMF}}\cdot\vec{\mu}_{\mathrm{e,IMF}}]^2 P(\Omega,t) \quad (12a)$$

$$A \propto \int_{\Omega_1} d\Omega_c \int_{\Omega_0} d\Omega \int_0^\infty dt\, f\left(\frac{t}{\sigma}\right) P(\Omega,t) \quad (13a)$$

where τ is the fluorescence lifetime, $\vec{n}_{\mathrm{IMF}}$ is the orientation of the emission analyzer, $\vec{\mu}_{\mathrm{e,IMF}}$ is the emission dipole, $f(t/\sigma)$ is the absorption relaxation function and σ the relaxation time for absorption, and Ω_1 is a domain appropriate for the Ω_c Euler angles. Absorption occurs on a time scale shorter than every other process under consideration so that $f(t/\sigma) \propto \delta(t)$. Following time integration and substitution from eq 11a

$$F \propto \int_{\Omega_1} d\Omega_c N(\Omega_c)\sum_j \frac{1}{\frac{1}{\tau}+\lambda_j} \times \int_{\Omega_0} d\Omega'[\vec{E}_{\mathrm{IMF}}(\Omega')\cdot\vec{\mu}_{\mathrm{a,IMF}}]^2\psi_j^*(\Omega') \times \int_{\Omega_0} d\Omega[\vec{n}_{\mathrm{IMF}}(\Omega)\cdot\vec{\mu}_{\mathrm{e,IMF}}]^2\psi_j \quad (14a)$$

$$A \propto \int_{\Omega_1} d\Omega_c N(\Omega_c)\int_{\Omega_0} d\Omega[\vec{E}_{\mathrm{IMF}}(\Omega)\cdot\vec{\mu}_{\mathrm{a,IMF}}]^2 \quad (15a)$$

We could introduce a model for the restricted independent movement of the probe and find expressions for ψ_j and λ_j for use in eq 14a. Alternatively, under the assumption that probe rotational relaxation is much faster than excited state relaxation, only the $j = 0$ term in the solution for $P(\Omega,t)$ survives, corresponding to a uniform distribution of probe within its allowed range of movement. Then eq 14a reduces to

$$F \propto \tau\int_{\Omega_1} d\Omega_c N(\Omega_c)\int_{\Omega_0} d\Omega'[\vec{E}_{\mathrm{IMF}}(\Omega')\cdot\vec{\mu}_{\mathrm{a,IMF}}]^2 \times \int_{\Omega_0} d\Omega[\vec{n}_{\mathrm{IMF}}(\Omega)\cdot\vec{\mu}_{\mathrm{e,IMF}}]^2 \quad (16a)$$

Equations 15a and 16a can be evaluated given $N(\Omega_c)$, Ω_b, the Euler angles (ϕ_1, θ, ϕ_2), and the angular domains Ω_0 and Ω_1.

The static angular distribution of cross-bridges in a muscle fiber, $N(\Omega_c)$, is uniform relative to rotation about the fiber axis but otherwise specifies myosin docked to actin. We introduce dispersion in cross-bridge orientation by evenly distributing the cross-bridge polar and torsional angles inside finite width domains. For a single, half-sarcomere

$$\int_{\Omega_1} d\Omega_c N(\Omega_c)\ldots \propto \int_0^{2\pi} d\alpha_c \int_{\beta_1-\beta_w}^{\beta_1+\beta_w} d\beta_c \sin\beta_c \int_{\gamma_1-\gamma_w}^{\gamma_1+\gamma_w} d\gamma_c \ldots \quad (17a)$$

where β_1 and γ_1 are from actoS1 coordinates (*19*) and β_w and γ_w are free parameters adjusted to improve agreement between calculated and observed signals.

The relationships between the PIF and the AMF (see eq 7a), specified by Euler angles Ω_b, relate the probe to the surrounding protein matrix and are the interesting free parameters constrained by all of the observed spectroscopic signals, including the polarization ratios and linear dichroism. The constraints are introduced by calculating the peak absorption energy, dipole and rotary strengths, and polarization ratios for fluorescein in F-S1 and comparing them to observed values. It is well established how this calculation gives fluorescein's absorption dipoles within the IMF (*21*). We determined fluorescein's emission dipole by requiring the relative orientation of the absorption and emission dipoles to reproduce the observed L-format polarization anisotropy, *r*, from immobilized and randomly oriented F-S1. Then

$$r \equiv \frac{F_{3,3} - F_{3,2}}{F_{3,3} + 2F_{3,2}} \tag{18a}$$

where F's are calculated from eq 16a with $N(\Omega_c) = 1$ and no independent probe movement. Data needed to fully specify the emission dipole orientation in space are the anisotropies from two or more absorption bands. These data are readily available for F-S1 (*34*).

Requiring r defined in eq 18a to reproduce values observed for F-S1 freely tumbling in solution determines the domain of independent probe movement, Ω_0. In this case calculated F's in eq 18a come from eq 16a with $N(\Omega_c) = 1$ and Ω_0 varied as a set of free parameters. There is no worry that S1 tumbling contributes to the fluorescence depolarization because the relaxation time for S1 movement is nearly 2 orders of magnitude longer than the fluorescein lifetime. Fast, on the order of nanoseconds or faster, local S1 conformational dynamics depolarizes fluorescence. This motion is indistinguishable from the independent probe movement in its effect on Ω_0.

We do not use linear dichroism here or in part 2 but foresee its potential application to muscle fibers decorated with TNP-S1. We modify eq 3a to make use of the quantity we know how to calculate in eq 15a that is only proportional to absorption using the total absorption A, such that

$$A = \frac{1}{3}(A_1 + A_2 + A_3) = \epsilon C l \tag{19a}$$

where ϵ is the extinction coefficient of the randomly oriented labeled protein, C is sample concentration, and l is the optical path length. Then eq 3a may be rewritten as

$$\frac{\Delta A}{A} = \frac{\epsilon_3 - \epsilon_1}{\epsilon} = 3\frac{A_3 - A_1}{A_1 + A_2 + A_3} \tag{20a}$$

The right-hand side of eq 20a is dependent on the probe orientation distribution from eq 15a. The left-hand side and middle expressions are experimentally observable.

REFERENCES

1. Maita, T., Yajima, E., Nagata, S., Miyanishi, T., Nakayama, S., and Matsuda, G. (1991) *J. Biochem. 110*, 75−87.
2. Rayment, I., Rypniewski, W. R., Schmidt-Base, K., Smith, R., Tomchick, D. R., Benning, M. M., Winkelmann, D. A., Wesenberg, G., and Holden, H. M. (1993) *Science 261*, 50−58.
3. Fisher, A. J., Smith, C. A., Thoden, J. B., Smith, R., Sutoh, K., Holden, H. M., and Rayment, I. (1995) *Biochemistry 34*, 8960−8972.
4. Gulick, A. M., Bauer, C. B., Thoden, J. B., and Rayment, I. (1997) *Biochemistry 36*, 11619−11628.
5. Smith, C. A., and Rayment, I. (1996) *Biochemistry 35*, 5404−5417.
6. Dominguez, R., Freyzon, Y., Trybus, K. M., and Cohen, C. (1998) *Cell 94*, 559−571.
7. Houdusse, A., Kalabokis, V. N., Himmel, D., Szent-Gyorgyi, A. G., and Cohen, C. (1999) *Cell 97*, 459−470.
8. Huxley, H. E. (1969) *Science 164*, 1356−1366.
9. Huxley, A. F., and Simmons, R. M. (1971) *Nature 233*, 533−538.
10. Spudich, J. A. (1994) *Nature 372*, 515−518.
11. Kitamura, K., Tokunaga, M., Iwane, A. H., and Yanagida, T. (1999) *Nature 397*, 129−134.
12. Botts, J., Thomason, J. F., and Morales, M. F. (1989) *Proc. Natl. Acad. Sci. U.S.A. 86*, 2204−2208.
13. Werber, M. M., Szent-Györgyi, A. G., and Fasman, G. D. (1972) *Biochemistry 11*, 2872−2883.
14. Nihei, T., Mendelson, R. A., and Botts, J. (1974) *Biophys. J. 14*, 236−242.
15. Schellman, J. A., and Jensen, H. P. (1987) *Chem. Rev. 87*, 1359−1399.
16. Edwards, R. A., and Woody, R. W. (1977) *Biochem. Biophys. Res. Commun. 79*, 470−476.
17. Towell, J. F., and Woody, R. W. (1980) *Biochemistry 19*, 4231−4237.
18. Burghardt, T. P., Park, S., and Ajtai, K. (2001) *Biochemistry 40*, 4834−4843.
19. Mendelson, R., and Morris, E. P. (1997) *Proc. Natl. Acad. Sci. U.S.A. 94*, 8533−8538.
20. Schellman, J. A., and Nielsen, E. B. (1967) *J. Phys. Chem. 71*, 3914−3921.
21. Bayley, P. M., Nielsen, E. B., and Schellman, J. A. (1969) *J. Phys. Chem. 73*, 228−243.
22. Burghardt, T. P., Garamszegi, S. P., Park, S., and Ajtai, K. (1998) *Biochemistry 37*, 8035−8047.
23. Ajtai, K., Peyser, Y. M., Park, S., Burghardt, T. P., and Muhlrad, A. (1999) *Biochemistry 38*, 6428−6440.
24. Burghardt, T. P., and Ajtai, K. (1994) *Biochemistry 33*, 5376−5381.
25. Ajtai, K., Toft, D. J., and Burghardt, T. P. (1994) *Biochemistry 33*, 5382−5391.
26. Geeves, M. A., and Holmes, K. C. (1999) *Annu. Rev. Biochem. 68*, 687−728.
27. Bagshaw, C. R., and Trentham, D. R. (1974) *Biochem. J. 141*, 331−349.
28. Werber, M. M., Peyser, Y. M., and Muhlrad, A. (1992) *Biochemistry 31*, 7190−7197.
29. Peyser, Y. M., Ajtai, K., Werber, M. M., Burghardt, T. P., and Muhlrad, A. (1997) *Biochemistry 36*, 5170−5178.
30. Goody, R. S., and Hofmann, W. (1980) *J. Muscle Res. Cell Motil. 1*, 101−115.
31. Brenner, B., Schoenberg, M., Chalovich, J. M., Green, L. E., and Eisenberg, E. (1982) *Proc. Natl. Acad. Sci. U.S.A. 79*, 7288−7291.
32. Tonomura, Y., Appel, P., and Morales, M. (1966) *Biochemistry 5*, 515−521.
33. Weeds, A. G., and Taylor, R. S. (1975) *Nature 257*, 54−56.
34. Ajtai, K., and Burghardt, T. P. (1992) *Biochemistry 31*, 4275−4288.
35. Borejdo, J., Putnam, S., and Morales, M. F. (1979) *Proc. Natl. Acad. Sci. U.S.A. 76*, 6346−6350.
36. Ajtai, K., Ilich, P. J. K., Ringler, A., Sedarous, S. S., Toft, D. J., and Burghardt, T. P. (1992) *Biochemistry 31*, 12431−12440.
37. Ajtai, K., and Burghardt, T. P. (1989) *Biochemistry 28*, 2204−2210.
38. Burghardt, T. P., and Ajtai, K. (1989) *Proc. Natl. Acad. Sci. U.S.A. 86*, 5366−5370.
39. Burghardt, T. P., Garamszegi, S. P., and Ajtai, K. (1997) *Proc. Natl. Acad. Sci. U.S.A. 94*, 9631−9636.
40. Ando, T. (1984) *Biochemistry 23*, 375−381.
41. Kinose, F., Wang, S. X., Kidambi, U. S., Moncman, C. L., and Winkelmann, D. A. (1996) *J. Cell Biol. 134*, 895−909.
42. Patterson, B., Ruppel, K. M., Wu, Y., and Spudich, J. A. (1997) *J. Biol. Chem. 272*, 27612−27617.
43. Berger, C. L., Craik, J. S., Trentham, D. R., Corrie, J. E. T., and Goldman, Y. E. (1996) *Biophys. J. 71*, 3330−3343.
44. Fisher, A. J., Smith, C. A., Thoden, J., Smith, R., Sutoh, K., Holden, H. M., and Rayment, I. (1995) *Biophys. J. 68*, 19s−28s.
45. Marcus, R. A., and Sutin, N. (1985) *Biochim. Biophys. Acta 811*, 265−322.
46. dos Remedios, C. G., Millikan, R. G. C., and Morales, M. F. (1972) *J. Gen. Physiol. 59*, 103−120.
47. Naylor, G. R. S., and Podolsky, R. J. (1981) *Proc. Natl. Acad. Sci. U.S.A. 78*, 5559−5563.
48. Aguirre, R., Gonsoulin, F., and Cheung, H. C. (1986) *Biochemistry 25*, 6827−6835.
49. Chandrasekhar, S. (1943) *Rev. Mod. Phys. 15*, 1−89.

BI002387O